Journal of Nuclear Materials 385 (2009) 517–526

Contents lists available at ScienceDirect

Journal of Nuclear Materials

journal homepage: www.elsevier.com/locate/jnucmat

The electrochemistry in 316SS crevices exposed to PWR-relevant conditions

M. Vankeerberghen [a,*], G. Weyns [b], S. Gavrilov [a], J. Henshaw [c], J. Deconinck [b]

[a] SCK•CEN, Boeretang 200, B-2400 Mol, Belgium
[b] VUB, Pleinlaan 2, B-1050 Brussels, Belgium
[c] NNL, Harwell International Business Centre, Didcot, Oxfordshire OX11 0QJ, United Kingdom

ARTICLE INFO

Article history:
Received 14 April 2008
Accepted 15 December 2008

ABSTRACT

The chemical and electrochemical conditions within a crevice of Type 316 stainless steel in boric acid–lithium hydroxide solutions under PWR-relevant conditions were modelled with a computational electrochemistry code. The influence of various variables: dissolved hydrogen, boric acid, lithium hydroxide concentration, crevice length, and radiation dose rate was studied. It was found with the model that 25 ccH_2/kg (STP) was sufficient to remain below an electrode potential of -230 mV_{she}, commonly accepted sufficient to prevent stress corrosion cracking under BWR conditions. In a PWR plant various operational B–Li cycles are possible but it was found that the choice of the cycle did not significantly influence the model results. It was also found that a hydrogen level of 50 ccH_2/kg (STP) would be needed to avoid substantial lowering of the pH inside a crevice.

1. Introduction

Type 316 stainless steel (SS316) is susceptible to stress corrosion cracking (SCC) in the coolant of pressurized-water nuclear reactors (PWRs) under some operational conditions [1]. Irradiation-assisted stress corrosion cracking (IASCC), a radiation-enhanced form of SCC, has been thought to be the cause of the failure of some core components in PWRs [2]. SCC initiation and propagation involves many physico-chemical processes in the material, the environment and their mutual interface (the oxide). In IASCC the phenomenon is further complicated for the environment (water) undergoes radiolysis and the material is subjected to microstructural and microchemical changes. In this paper the effect of water radiolysis on the local crevice conditions (electrode potential, oxidizing species concentration and pH) is investigated using a sophisticated finite element model.

(IA)SCC is most likely to occur in occluded regions, i.e. regions with a reduced mass transport due to limited convection and which are likely to develop a local electrochemistry different from the bulk. Indeed, baffle bolt failures in PWRs have been attributed to corrosion in creviced environments [3]. Local electrochemical conditions and temperature play an important role and these are influenced by species transport through the occluded region. In view of the difficulties associated with measuring local electrochemical conditions in crevices and cracks and in order to understand SCC initiation and propagation it is important to study the local electrochemical conditions in occluded regions through computations. The difficulty of carrying out such measurements in a radiation environment makes the need for calculations even greater. ECHEM is a computational electrochemistry code written to evaluate the electrochemical conditions within crevices open to PWR chemistry. The code and the results of using it for typical PWR conditions are described in this article.

2. The electrochemical model

In order to calculate local electrochemical conditions within occluded regions, one has to model the transport and chemistry of the various chemical species in the geometry of the crevice [4]. The transport of species is affected by fluid flow (species are transported by convection), electro-migration (charged species are transported in a potential gradient) and diffusion (species are transported in a concentration gradient). In addition the many homogeneous reactions within the coolant and heterogeneous reactions on the metal surfaces need to be modelled. All these processes have been described in terms of mathematical equations. The resulting set of equations is heavily coupled and need to be solved simultaneously. The following is a brief description of the species, chemistry and equations used in the present model.

2.1. Model geometry

For the calculations discussed here rectangular, two-dimensional crevice geometry was assumed, as shown in Fig. 1. The crevice is placed to the side of a channel, halfway between the channel inlet at the bottom and the channel outlet at the top. The channel width is five times the crevice width and its height is four times the crevice width at each side of the crevice. The crevice is assumed to be clean and free of corrosion product (crud) built-up.

* Corresponding author. Tel.: +32 14 33 31 82; fax: +32 14 32 12 16.
E-mail address: marc.vankeerberghen@sckcen.be (M. Vankeerberghen).

0022-3115/$ - see front matter © 2009 Elsevier B.V. All rights reserved.
doi:10.1016/j.jnucmat.2008.12.175

Nomenclature

Physical constant

F	Faraday's constant (96,500) (C/mol)
R	universal gas constant (8.31441) (J/mol/K)

Calculated variables

p	hydrostatic pressure
v	water velocity (m/s)
C	concentration (mol/m^3)
E	electrode potential (V)
U	solution potential (V)

Input parameters

T	temperature (K)
T_c	temperature (°C)
L	crevice length (m)
W	crevice width (m)
AR	crevice aspect ratio (–)
$\Phi_{\gamma,n,\alpha}$	gamma, neutron, alpha dose rates (Mrad/h)

Model parameters/properties

ρ	water density (kg/m^3)
μ	water dynamic viscosity (kg/m/s)
z	charge (–)
α	electrode transfer coefficient (–)
λ	equivalent conductivity (Scm^2)
D	diffusion coefficient (m^2/s)
k	reaction rate (varying)

2.2. Model chemistry

Six homogeneous reactions are associated with the aqueous boric acid–lithium hydroxide solution. The reactions and their temperature dependent rate constants are listed in Table 1. The nine species involved in these reactions are: H^+, OH^-, $B(OH)_3$, $B(OH)_4^-$, $B_2(OH)_7^-$, $B_3(OH)_{10}^-$, $Li(OH)$, Li^+, $LiB(OH)_4$.

Two homogeneous reactions associated with metal hydrolysis are included in the model. The reactions and their rate constants are listed in Table 2. The additional species involved in these reactions are M^{2+}, $M(OH)^+$.

Irradiation (gamma, alpha and neutron fluxes) of water produces various radiolytic species. In this study we consider e^-, H^+, OH, H, H_2 and H_2O_2. The production rates of these primary species are given in Table 3. In general, these species undergo a number of radiolytic reactions, of which there are probably 40–50. The inclusion of such a large number of reactions and species within a finite element model of the type described here is computationally expensive. For this reason a separate sensitivity study was carried out to identify a smaller subset of species and rate equations that could be used to model the radiolysis chemistry under the limited range of PWR conditions considered here. This study gave the radiolytic reactions and their rate constants listed in Table 4 and in general the difference between using the full chemistry and this reduced chemistry only amounted to 5–10% errors in predicted bulk concentrations of the main oxidants for typical PWR conditions.

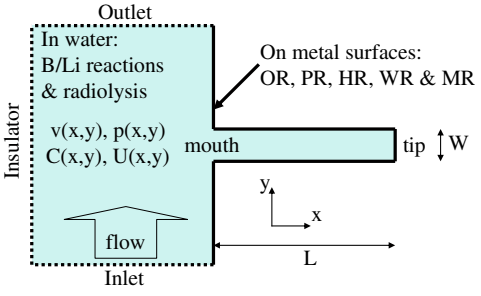

Fig. 1. Schematic drawing of the crevice geometry and the processes in ECHEM. The electrode reactions OR, PR, HR, WR and MR are listed in Table 6.

2.3. Transport equations

Transport of ionic and dissolved species in the environment is modelled using dilute solution theory [5]. This leads to the Nernst–Planck equation describing transport due to diffusion, electro-migration and convection, for every species i, i.e.

$$\vec{N}_i = -D_i\vec{\nabla}C_i - \frac{F}{RT}z_iD_iC_i\vec{\nabla}U + C_i\vec{v} \quad \forall i, \tag{1}$$

where subscript i refers to the species' number, $\vec{N}_i$ is the flux in mol/m^2/s, C_i is the concentration in mol/m^3, z_i the charge, D_i the diffusion coefficient in m^2/s, U the solution potential in V and $\vec{v}$ the flow

Table 2
Hydrolysis reactions and their rate constants (assumed).

Reaction	Rate constant k_f for concentrations in mol/m^3
$M^{2+} + OH^- \rightarrow M(OH)^+$	$k_f = 10^5$
$M(OH)^+ + OH^- \rightarrow M(OH)_2\downarrow$	$k_f = 10^5$

Table 1
Boric acid–lithium hydroxide reactions and their rates [11].

Reaction	Rate constants k_f and k_b concentrations in mol/kg, temperature T_c in °C and T in K and density in kg/m^3
$B(OH)_3 + OH^- \Longleftrightarrow B(OH)_4^-$	$k_f = Q_1/\rho$ where $Q_1 = 10^{pQ_1}$; $k_b = 1$
$B(OH)_4^- + B(OH)_3 \Longleftrightarrow B_2(OH)_7^-$	$k_f = P_2/\rho$ where $P_2 = Q_2/Q_1$ and $Q_2 = 10^{pQ_2}$; $k_b = 1$
$B_2(OH)_7^- + B(OH)_3 \Longleftrightarrow B_3(OH)_{10}^-$	$k_f = P_3/\rho$ where $P_3 = Q_3/Q_2$ and $Q_3 = 10^{pQ_3}$; $k_b = 1$
$Li^+ + OH^- \Longleftrightarrow Li(OH)$	$k_f = Q_6/\rho$ where $Q_6 = 10^{pQ_6}$; $k_b = 1$
$Li^+ + B(OH)_4^- \Longleftrightarrow LiB(OH)_4$	$k_f = Q_7/\rho$ where $Q_7 = 10^{pQ_7}$; $k_b = 1$
$H_2O \Longleftrightarrow H^+ + OH^-$	$k_f = k_b\,K_w\,\rho^2$ where $K_w = 10^{pK_w}$; $k_b = 6.62\ 10^{10} + 1.48 \times 10^9 T_c + 1.28 \times 10^7 T_c^2 - 6.03 \times 10^4 T_c^3 + 128 T_c^4$
$pQ_1 = 1573.21/T + 28.6059 + 0.012078\,T - 13.2258\log_{10}(T)$	
$pQ_2 = 2756.1/T - 18.966 + 5.835\log_{10}(T)$	
$pQ_3 = 3339.5/T - 8.084 + 1.497\log_{10}(T)$	
$pQ_6 = \log_{10}(1.99)$	
$pQ_7 = \log_{10}(2.12)$	
$pK_w = -4.098 - 3245.2/T + 2.2363 \times 10^5/T^2 - 3.9984 \times 10^7/T^3 + (13.957 - 1262.3/T + 8.5641 \times 10^5/T^2)\log(\rho/1000)$	

Table 3
Radiolytic production rates.

Radiation production rates in mol/L/s for Φ in Mrad/h
$DR_{e^-} = 2.87 \times 10^{-7}(3.6\Phi_\gamma + 0.65\Phi_n + 0.05\Phi_\alpha)$
$DR_{H^+} = 2.87 \times 10^{-7}(3.6\Phi_\gamma + 0.65\Phi_n + 0.05\Phi_\alpha)$
$DR_H = 2.87 \times 10^{-7}(0.8\Phi_\gamma + 0.3\Phi_n + 0.16\Phi_\alpha)$
$DR_{OH} = 2.87 \times 10^{-7}(5.0\Phi_\gamma + 2.0\Phi_n + 0.56\Phi_\alpha)$
$DR_{H_2} = 2.87 \times 10^{-7}(0.65\Phi_\gamma + 1.225\Phi_n + 1.605\Phi_\alpha)$
$DR_{H_2O_2} = 2.87 \times 10^{-7}(0.35\Phi_\gamma + 0.70\Phi_n + 1.43\Phi_\alpha)$ [18]

velocity in m/s. R, F and T have their usual meaning. Conservation of mass requires that

$$\frac{\partial C_i}{\partial t} = -\vec{\nabla}\vec{N}_i + \sum_k R_{k,i} \quad \forall i, \tag{2}$$

where $R_{k,i}$ is the production rate of species i in reaction k. One additional equation, the Poisson equation, is needed to solve for the solution potential, i.e.

$$\nabla^2 U = -\frac{F}{\varepsilon}\sum_{i=1}^{n} z_i C_i, \tag{3}$$

where ε is the permittivity of the solution in $C^2/(Nm^2)$. The temperature and viscosity dependent diffusion coefficients for the various species are listed in Table 5. The conductivity κ of the solution can be calculated on the basis of the Nernst–Einstein relation:

$$\kappa = \frac{F^2}{RT}\sum_{i=1}^{n} z_i^2 D_i C_i. \tag{4}$$

The full system of $n + 1$ equations, where n is the number of species in the solution, is solved using a finite element code [6] and yields the concentrations C_i and the solution potential U in the electrochemical system.

Table 4
Radiolytic reactions and their rate constants.

Radiolysis reactions [19]	Rate constants k_f and k_b for concentrations in mol/L temperature T_c in °C and T in K and density in kg/m^3
$OH + H_2 \rightarrow H + H_2O$	$k_f = 6.31 \times 10^{10}\ \exp(-18150/RT)$
$e^- + H_2O \Longleftrightarrow H + OH^-$	$k_f = k_{-2}\ K_w\ \rho^2\ 10^{pK_H}$ $k_b = 1.33 \times 10^{14}\ \exp(-38380/RT)$
$e^- + H_2O_2 \rightarrow OH + OH^-$	$k_f = 6.94 \times 10^{12}\ \exp(-15360/RT)$
$OH + H_2O_2 \rightarrow HO_2 + H_2O$	$k_f = 1.47 \times 10^{10}\ \exp(-15620/RT)$
$OH + HO_2 \rightarrow O_2 + H_2O$	$k_f = 1.04 \times 10^{11}\ \exp(-5620/RT)$
$2OH \rightarrow H_2O_2$	$k_f = 1.0 \times 10^{11}\ \exp(-7650/RT)$
$e^- + OH \rightarrow OH^-$	$k_f = 7.39 \times 10^{11}\ \exp(-7920/RT)$
$HO_2 \Longleftrightarrow O_2^- + H^+$	$k_f = k_{-8}\ 10^{-pK_{HO_2}}$ $k_b = 3.41 \times 10^{10} + 2.75 \times 10^8 T_c + 1.24 \times 10^7\ T_c^2 - 6.23 \times 10^4 T_c^3 + 131 T_c^4$
$HO_2 + O_2^- + H_2O \rightarrow H_2O_2 + O_2 + OH^-$	$k_f = 2.44 \times 10^9\ \exp(-8600/RT)$
$O_2^- + OH \rightarrow OH^- + O_2$	$k_f = 8.75\ 10^{11}\ \exp(-10850/RT)$
$O_2 + e^- \rightarrow O_2^-$	$k_f = 5.44\ 10^{12}\ \exp(-14170/RT)$
$O_2 + H \rightarrow HO_2$	$k_f = 9.57\ 10^{11}\ \exp(-10610/RT)$
$2e^- + 2H_2O \rightarrow H_2 + 2OH^-$	$k_f = 2.33\ 10^{13}\ \exp(-20300/RT)$
$H + H_2O_2 \rightarrow OH + H_2O$	$k_f = 3.21\ 10^{10}\ \exp(-15940/RT)$
$HO_2 + OH^- \Longleftrightarrow O_2^- + H_2O$	$k_f = 7.22\ 10^9 + 1.62\ 10^8\ T_c + 2.4\ 10^6\ T_c^2 - 7.81\ 10^3\ T_c^3 + 10.6\ T_c^4$ $k_b = k_{15}\ K_w\ \rho^2\ 10^{-pK_{HO_2}}$
$e^- + O_2^- + 2H_2O \rightarrow H_2O_2 + 2OH^-$	$k_f = 3.1\ 10^{12}\ \exp(-13600/RT)$

$pK_H = 10.49 - 4.103 \times 10^{-2} T_c + 1.433 \times 10^{-4} T_c^2 - 2.325 \times 10^{-7} T_c^3 + 2.065 \times 10^{-10} T_c^4$.
$pK_{HO_2} = 4.917 - 3.813 \times 10^{-3} T_c + 8.771 \times 10^{-7} T_c^2 + 2.177 \times 10^{-7} T_c^3 - 4.0 \times 10^{-10} T_c^4$.

Table 5
Diffusion coefficients for ionic (a), dissolved (b) and neutral & radiolytic (c) species in an irradiated boric acid – lithium hydroxide solution.

(a) [12]

Ionic species	z	Specific conductance λ^{298K} - S cm^2/equiv
H^+	1	350
OH^-	−1	199
$B(OH)_4^-$	−1	40
$B_2(OH)_7^-$	−1	34
$B_3(OH)_{10}^-$	−1	27
Li^+	1	39
M^{2+}	2	39
$M(OH)^+$	1	39

From specific conductance to diffusion coefficient $D^T = \frac{1}{10}\frac{\lambda^{298K}}{z^2}\frac{\mu_{298K}}{\mu_T}\frac{T}{298}\frac{RT}{\rho F^2}$ (T in K)

(b) [13]

Dissolved species – D^T - m^2/s (T in K)	
O_2	$8.03 \times 10^{-7} e^{(-14600/RT)}$
H_2	$10^{-4} e^{(-5.700267 - 296.7439/T - 288379.2/T^2)}$
H_2O_2	$8.03 \times 10^{-7} e^{(-14600/RT)}$

(c)

Neutral and radiolytic species	D^{298K} - m^2/s
H_2O	1°
$B(OH)_3$	2.0×10^{-9}*
$Li(OH)$	2.0×10^{-9}*
$LiB(OH)_4$	2.0×10^{-9}*
e^-	2.0×10^{-9}*
O_2^-	2.0×10^{-9}*
H	2.0×10^{-9}*
OH	2.0×10^{-9}*
HO_2	2.0×10^{-9}*

$D^T = D^{298K}\frac{\mu_{298k}}{\mu_T}\frac{T}{298}$ (T in K)

* Our estimate, no literature values found.
° Value much larger than all other to ensure availability.

2.4. Fluid flow

The fluid flow is modelled using the incompressible Navier–Stokes and the continuity equations

$$\rho(T)\left(\frac{\partial \bar{v}}{\partial t} + (\bar{v}\cdot\bar{\nabla})\cdot\bar{v}\right) = \mu(T)\bar{\nabla}^2\bar{v} - \bar{\nabla}p, \tag{5}$$

$$\bar{\nabla}\cdot\bar{v} = 0, \tag{6}$$

where ρ is the water density in kg/m^3, p is the hydrostatic pressure in Pa, v the velocity in m/s and μ the dynamic viscosity in kg/m/s. The solution of these equations, for a given temperature, yields the velocity $\bar{v}$ and pressure ρ at each point. The inlet flow conditions are given in the form of a Reynolds number defined as follows

$$Re = \frac{\rho v L}{\mu}, \tag{7}$$

where L is a characteristic length in m and v the velocity in the centre of the flow channel in m/s. In the simulations a Re of 1000 gives a typical velocity of about 0.5 m/s in the middle of the channel.

2.5. Boundary conditions

Fully developed laminar flow, hence a parabolic velocity profile, is assumed at the inlet to the channel. At the outlet of the channel a constant back pressure is assumed. Along the channel and crevice walls the velocity is set to zero. After solution, the flow field is parabolic throughout the domain, except at the crevice mouth. Into the crevice the velocity tends rapidly to zero.

All metallic walls (thick solid lines in Fig. 1), internal and external to the crevice, are considered to be 316 stainless steel and five electrode reactions, the hydrogen reaction (HR), the oxygen reaction

Table 6
Electrode reactions and their associated current density. Current density and local concentration are, respectively, expressed in A/m^2 and mol/m^3. E the local electrode potential (V_{she}) and F, R and T has their usual meaning.

Label	Reaction	Current density
HR	$2H^+ + 2e^- \Longleftrightarrow H_2$	$i_{HR} = 1.682[H_2]e^{\left(\frac{2.0.999EF}{RT}\right)} - 7.89\times10^{-4}[H^+]e^{\left(-\frac{2.0.45EF}{RT}\right)}$ [14]
OR	$O_2 + 4e^- + 2H_2O \rightarrow 4OH^-$	$i_{OR} = -0.18[O_2]^{0.66}e^{\left(-\frac{4.0.17FE}{RT}\right)}$ (adapted from [15])
PR	$H_2O_2 + 2e^- \rightarrow 2OH^-$	$i_{PR} = -150[H_2O_2]^{0.84}e^{\left(-\frac{2.0.35FE}{RT}\right)}$ (adapted from [16])
WR	$2H_2O + 2e^- \rightarrow 2OH^- + H_2$	$i_{WR} = -7.5\times10^{-8}e^{\left(-\frac{2.0.57FE}{RT}\right)}$ [17]
MR	$M + M^{2+} + 2e^-$	$i_{MR} = 0.012$ (adapted from [13], assumed T-independent)

Table 7
Input parameters and ranges for ECHEM.

Parameter	Unit	Abbreviation	Range	Default
Crevice length	μm	L	(10–100000)	100
Crevice width	μm	W	(10–100000)	10
Boric acid concentration	ppm	B	(0–5000)	1000
Lithium hydroxide concentration	ppm	Li	(0–10)	2
Dissolved hydrogen concentration	cc/kg	H_2	(0–50)	25
Alpha dose rate	Mrad/h	Φ_α	(0–5000)	2175
Gamma dose rate	Mrad/h	Φ_γ	(0–5000)	1200
Neutron dose rate	Mrad/h	Φ_n	(0–5000)	2400
Temperature	°C	T	(25–350)	300
Reynolds number	–	Re	(0–2000)	1000

(OR), the hydrogen-peroxide reaction (PR), the water reduction reaction (WR) and the metal dissolution reaction (MR) are assumed to occur in parallel on a natural oxide layer. The simultaneously operating electrode reactions and the corresponding expressions for their current density are given in Table 6. The species fluxes at the metallic walls are directly associated with these expressions. At the channel inlet equilibrium concentrations and zero solution potential are imposed. At the channel outlet zero normal gradients in concentration and potential are assumed, i.e. purely convective conditions. At the left edge of the domain zero normal species flux and current density are assumed, i.e. insulator conditions.

3. Computer program

ECHEM (ElectroCHEMistry) is a finite element-based tool for the calculation of the electrochemistry in 2D, rectangular, stainless steel crevices exposed to a boric acid–lithium hydroxide solution under PWR-relevant conditions, including reduced reaction-set radiolysis. The advantage of using a finite element solution technique is the separation between model specification (which for a given material and environment stays fixed) and geometry (which can be arbitrary). The program has been designed with a user friendly interface. The input screen restricts the user's input to the parameters listed in Table 7. The inputs concern geometry (crevice length and width), chemistry (boric acid, lithium hydroxide and dissolved hydrogen concentrations), radiolysis (alpha, gamma and neutron dose rates) and thermo-hydraulic conditions (temperature and flow). Output from the program includes both contour plots and line plots, the results presented in this paper corresponding to typical output. The calculations proceed in the following way. First two grids are generated, one for the computation of the flow field and another for the computation of the electrochemistry. Then the flow field is calculated and interpolated on the electrochemistry grid. Subsequently the equilibrium chemical conditions are calculated and imposed at the channel inlet. Finally the electrochemical conditions inside the full domain are calculated.

4. Results

The model has been used to investigate various sensitivities to typical input parameters such as the crevice length L, the total boron [B] and lithium [Li] concentrations, the dissolved hydrogen concentration [H_2], the radiolytic production rates DR_α, DR_γ and DR_n, the temperature T and the Reynolds number Re. The results are analysed in terms of electrode potential (OCP, E_{mouth}, E_{tip}), pH (pH_{mouth}, pH_{tip}), dissolved hydrogen concentration ($H_{2,\text{mouth}}$, $H_{2,\text{tip}}$), dissolved oxygen concentration ($O_{2,\text{mouth}}$, $O_{2,\text{tip}}$) and hydrogen-peroxide concentration ($H_2O_{2,\text{mouth}}$, $H_2O_{2,\text{tip}}$).

Initially the crevice aspect ratio (AR = length/width = 30, 100, 200, 500), the hydrogen concentration in the primary water (0.01, 0.1, 0.15, 0.2, 0.25, 0.3, 1, 10, 25, 30, 50 ccH_2/kg STP) and the radiation level (half, nominal, factor of 2 increase) were changed. The other input parameters were kept constant at 1000 ppmB, 2 ppmLi, 300 °C, Re = 1000 and W = 10 μm. The results are presented in Figs. 2–9. All graphs show one of the calculated variables as a function of the primary water hydrogen concentration for various crevice aspect ratios (30, 100, 200, 500) and radiation levels (0.5, 1, 2). The calculated variables are, respectively, the corrosion potential (Fig. 2), the potential drop inside the crevice (Fig. 3) the electrode potential at the crevice tip (Fig. 4), the pH drop inside the crevice (Fig. 5), the dissolved oxygen (Fig. 6) and hydrogen-peroxide (Fig. 7) concentrations at the crevice mouth and the dissolved hydrogen concentration at the crevice mouth (Fig. 8) and tip (Fig. 9).

In a second exercise the concentrations of boric acid and lithium hydroxide were changed according to two typical PWR operational cycles [8] (Fig. 10) for two crevice aspect ratios (AR = L/W = 100, 500). In the first operational cycle the pH is kept constant as the total boron content is decreased and the total lithium content is adapted accordingly. In the second operational cycle the total lithium content is kept constant as the total boron content is decreased until the pH reaches 7.4 after which the pH is kept constant at 7.4. The symbols in Fig. 10 (diamonds for cycle 1 and triangles for cycle 2) indicate the points for subsequent calculations along the two cycles. The other input parameters were kept constant with a typical radiation level, 25 cc/kg STP H_2, a temperature of 300 °C, a Reynolds number of 1000 and a crevice width of 10 μm. The results are presented in Figs. 11–15. All graphs show one of the calculated variables as a function of the boric acid concentration into the cycle for the two crevice aspect ratios. The calculated variables are, respectively, the corrosion potential (Fig. 11) and the electrode potential (Fig. 12), pH (Fig. 13), hydrogen-peroxide (Fig. 14) and dissolved hydrogen concentrations (Fig. 15) at the crevice mouth and tip. Arrows indicate the magnitude of the drops/increments from crevice mouth to tip.

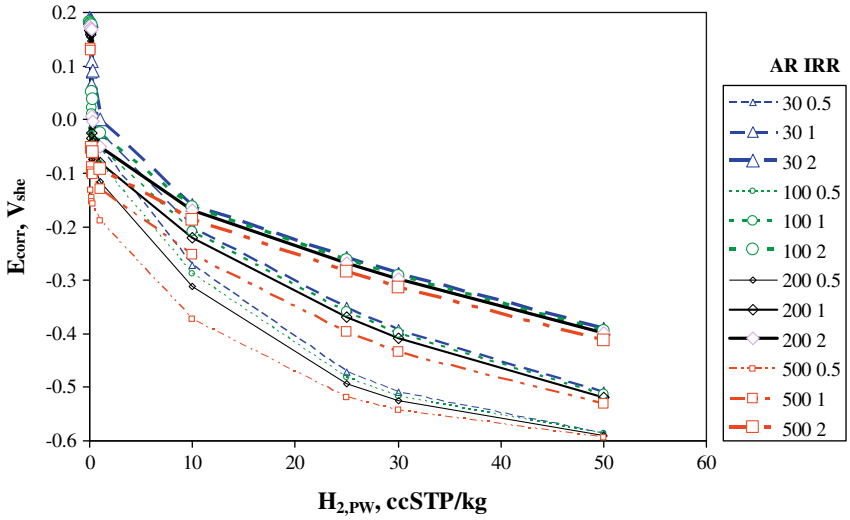

Fig. 2. Corrosion potential as a function of the primary water hydrogen concentration for various crevice aspect ratios (30, 100, 200, 500) and radiation levels (0.5, 1, 2); 1000 ppmB, 2 ppmLi, 300 °C, *Re* = 1000 and *W* = 10 μm.

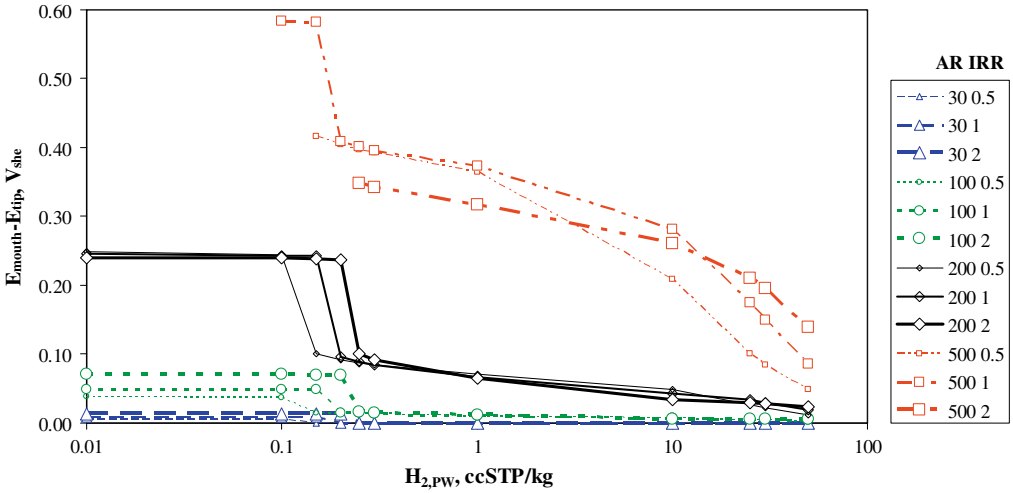

Fig. 3. Potential drop inside the crevice as a function of the primary water hydrogen concentration for various crevice aspect ratios (30, 100, 200, 500) and radiation levels (0.5, 1, 2); 1000 ppmB, 2 ppmLi, 300 °C, *Re* = 1000 and *W* = 10 μm.

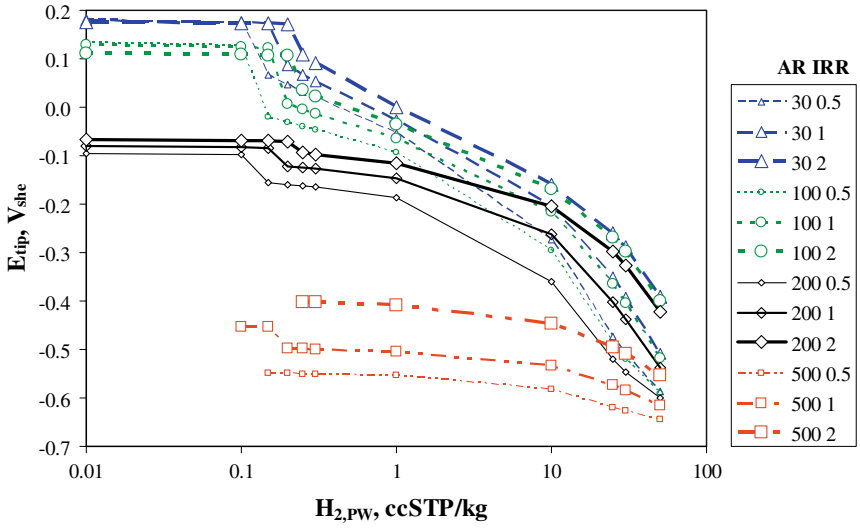

Fig. 4. Electrode potential at the crevice tip as a function of the primary water hydrogen concentration for various crevice aspect ratios (30, 100, 200, 500) and radiation levels (0.5, 1, 2); 1000 ppmB, 2 ppmLi, 300 °C, *Re* = 1000 and *W* = 10 μm.

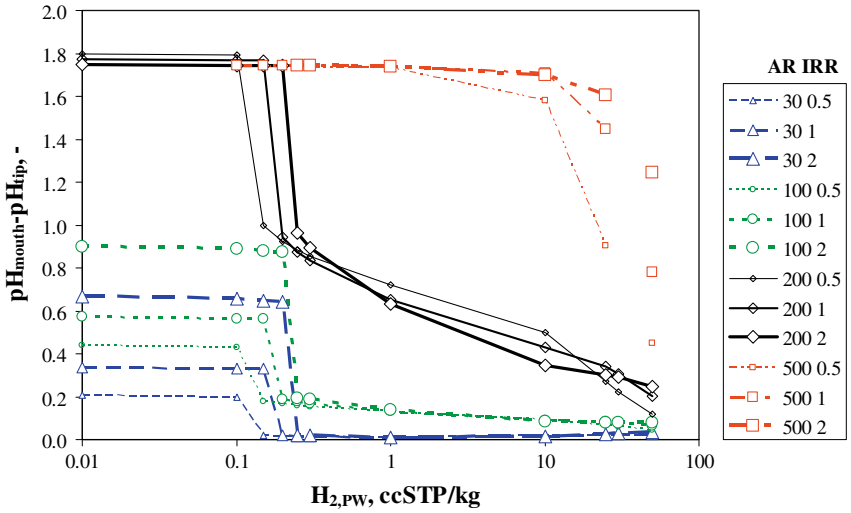

Fig. 5. pH drop inside the crevice as a function of the primary water hydrogen concentration for various crevice aspect ratios (30, 100, 200, 500) and radiation levels (0.5, 1, 2); 1000 ppmB, 2 ppmLi, 300 °C, Re = 1000 and W = 10 μm.

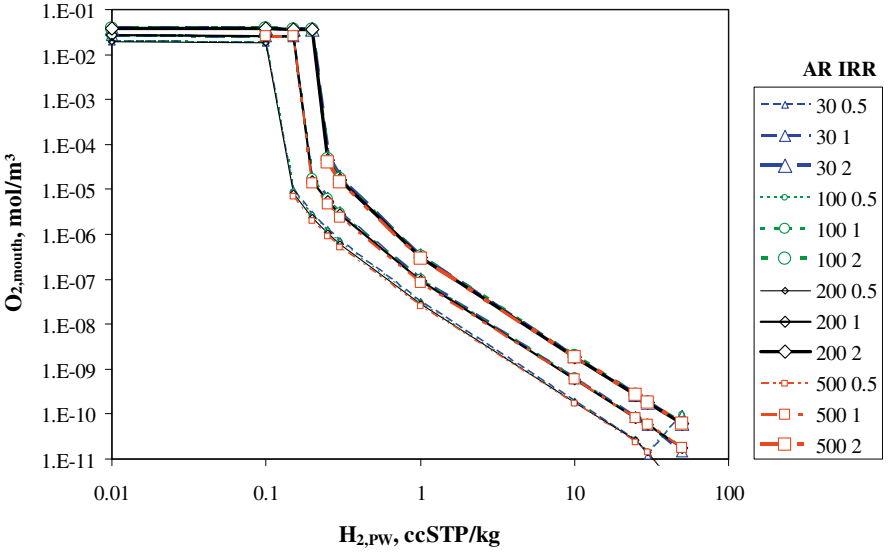

Fig. 6. Dissolved oxygen concentration at the crevice mouth as a function of the primary water hydrogen concentration for various crevice aspect ratios (30, 100, 200, 500) and radiation levels (0.5, 1, 2); 1000 ppmB, 2 ppmLi, 300 °C, Re = 1000 and W = 10 μm.

5. Discussion

In setting up the sensitivity studies we defined the aspect ratio AR as crevice length over crevice width (L/W). This is not necessarily a correct scaling factor, as crevices rather scale as the crevice length over the square of the height (L/W^2). However, once homogeneous reactions are involved also the aspect ratio L/W^2 will not be applicable any longer. Hence, our aspect ratio change is actually a variation of the crevice length at a given crevice width of 10 μm.

5.1. Effect of primary water hydrogen, aspect ratio and radiation level

Fig. 2 shows the corrosion potential as a function of the primary water hydrogen concentration for various crevice aspect ratios and radiation levels. It is apparent that the corrosion potential is influenced by the radiation dose rate level. The corrosion potential decreases with the primary water hydrogen concentration and increases with the radiation level. The graphs illustrate the suppression of radiolysis by primary water hydrogen. It also shows that the corrosion potential is not affected by the presence of a crevice up to an aspect ratio of 100. However, at an aspect ratio of 500 the corrosion potential is affected. This seems logical for the metallic surface area ratio between the crevice internal and external environment is being changed.

Fig. 3 shows the potential drop inside the crevice (mouth–tip) as a function of the primary water hydrogen concentration for various crevice aspect ratios and radiation levels. The potential drop decreases with the primary water hydrogen concentration and increases with the crevice aspect ratio. The slope depends on the radiation dose rate. For the largest crevice aspect ratio, AR = 500, there is a marked decrease of the slope with the radiation dose rate. The higher the dose rate the weaker the slope and the less sensitive the potential drop is to the primary water hydrogen concentration, yielding a higher potential drop at high primary water hydrogen concentrations.

Fig. 4 shows the electrode potential at the crevice tip as a function of the primary water hydrogen concentration for various crevice aspect ratios and radiation levels. The electrode potential

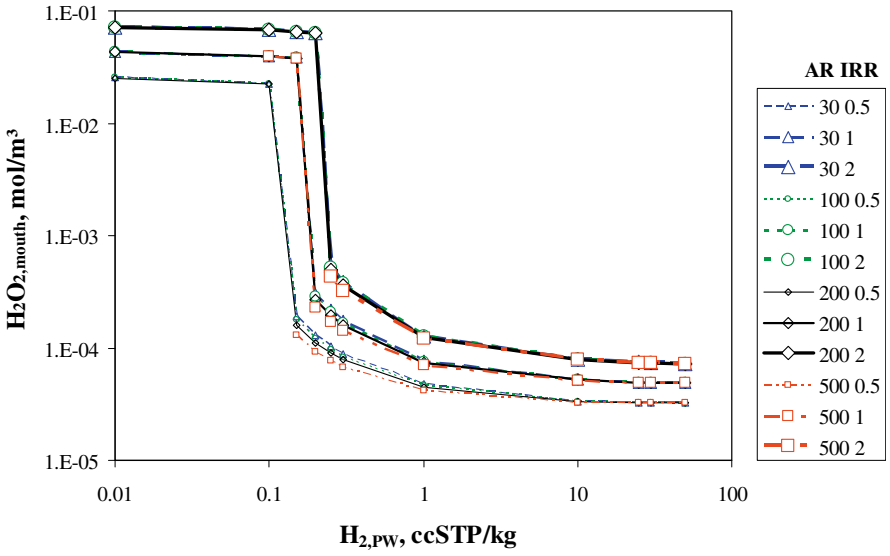

Fig. 7. Hydrogen-peroxide concentration at the crevice mouth as a function of the primary water hydrogen concentration for various crevice aspect ratios (30, 100, 200, 500) and radiation levels (0.5, 1, 2); 1000 ppmB, 2 ppmLi, 300 °C, *Re* = 1000 and *W* = 10 μm.

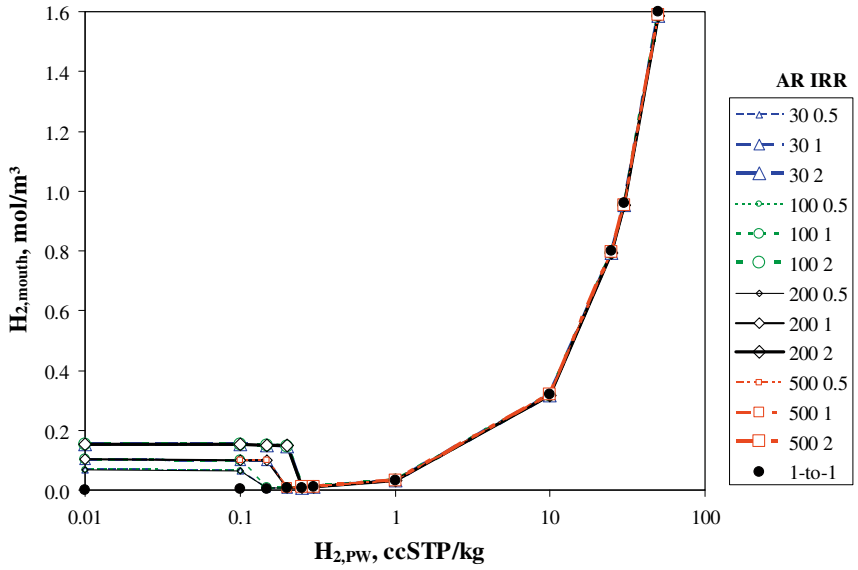

Fig. 8. Dissolved hydrogen concentration at the crevice mouth as a function of the primary water hydrogen concentration for various crevice aspect ratios (30, 100, 200, 500) and radiation levels (0.5, 1, 2); 1000 ppmB, 2 ppmLi, 300 °C, *Re* = 1000 and *W* = 10 μm.

decreases with the primary water hydrogen concentration and the crevice aspect ratio and increases with the radiation level. The conditions at the tip are particularly important in respect of stress corrosion cracking for they determine the driving force for crevice or crack advance [7]. Hence, a high primary water hydrogen concentration and a long crevice are beneficial for they both lower the electrode potential at the tip. The beneficial effect of a long crevice somewhat disappears at higher primary water hydrogen concentration.

Fig. 5 shows the pH drop inside the crevice (mouth–tip) as a function of the primary water hydrogen concentration for various crevice aspect ratios and radiation levels. The external pH and pH at the crevice mouth are close to each other and constant. Hence the figures are presented as pH drops. The pH drop decreases with the primary water hydrogen concentration and increases with the crevice aspect ratio. The slope of the decrease with the primary water hydrogen concentration depends on the dose rate. For the largest crevice aspect ratio there is a marked decrease of the slope with the dose rate. The higher the radiation level the weaker the slope. This is associated with the relative proportion of proton production by radiolysis and hydrolysis. The calculations show that at low primary water hydrogen concentration, where radiolysis is not suppressed, the pH drops by about half a unit (two units) from crevice mouth to tip in a 1 mm (5 mm) long crevice (ARs = 100, 500).

Figs. 6 and 7 show the dissolved oxygen and hydrogen-peroxide concentrations at the crevice mouth as a function of the primary water hydrogen concentration for various crevice aspect ratios and radiation levels. The concentration of the oxidizing species is independent of the crevice length and decreases with the primary water hydrogen concentration and increases with the radiation level. Radiolysis is effectively being suppressed in the environment from a primary water hydrogen concentration of 0.1–1 ccH_2/kg,

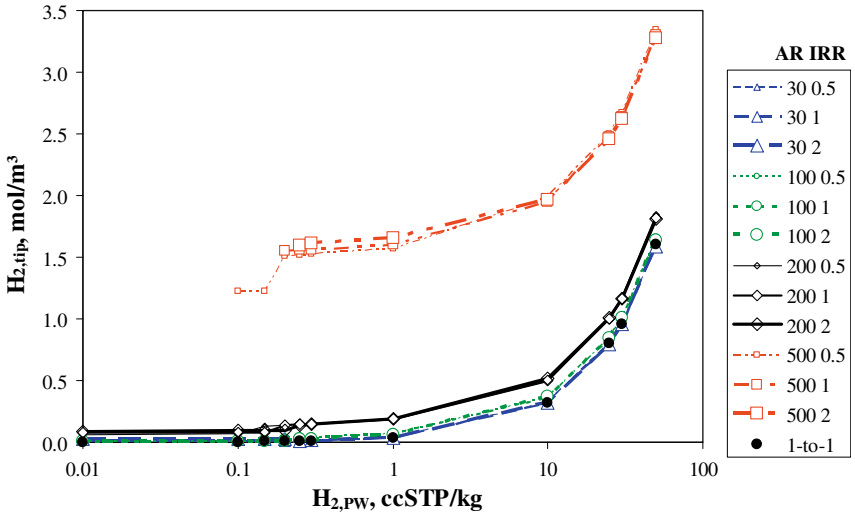

Fig. 9. Dissolved hydrogen concentration at the crevice tip as a function of the primary water hydrogen concentration for various crevice aspect ratios (30, 100, 200, 500) and radiation levels (0.5, 1, 2); 1000 ppmB, 2 ppmLi, 300 °C, *Re* = 1000 and *W* = 10 μm.

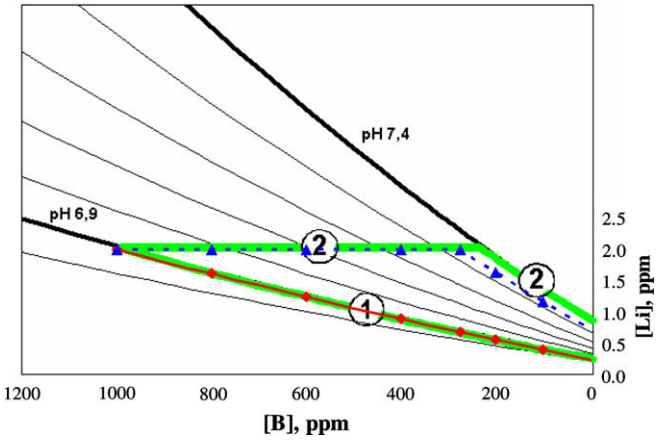

Fig. 10. Two operational boric acid – lithium hydroxide cycles. (1) A cycle with a constant pH. (2) A cycle with a constant lithium content until a pH of 7.4 is reached [8].

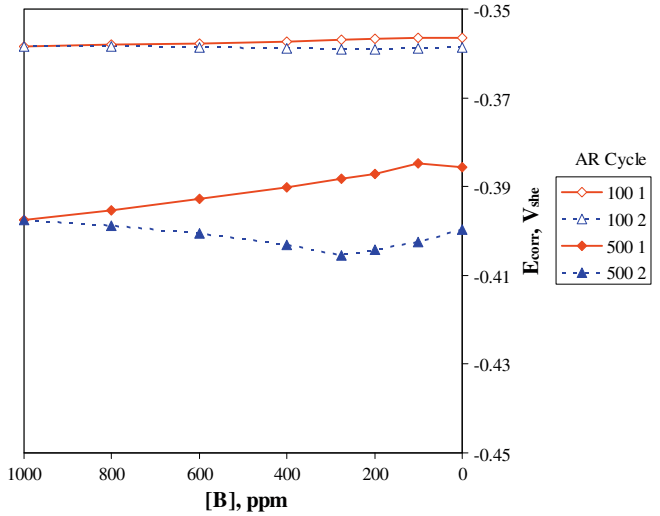

Fig. 11. Corrosion potential as a function of boric acid concentration for two crevice aspect ratios (100 and 500) and two operational cycles (1 and 2). Nominal radiation level, 25 ccH_2/kg, 300 °C, *Re* = 1000 and *W* = 10 μm.

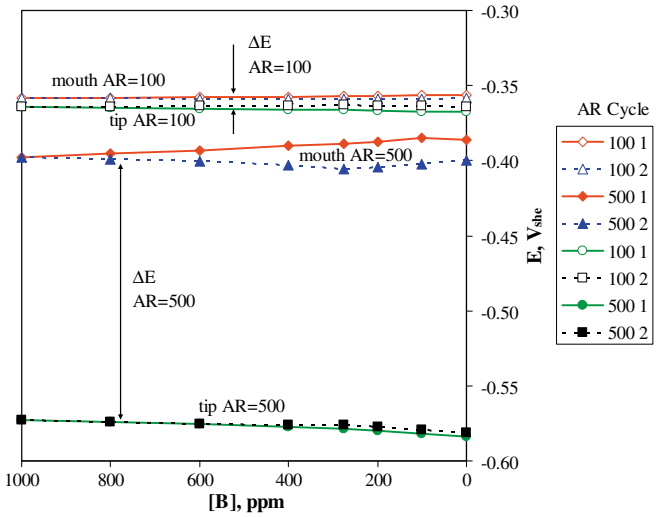

Fig. 12. Electrode potential at the crevice mouth (diamonds and triangles) and tip (circles and squares) as a function of boric acid concentration for two crevice aspect ratios (100, open symbols and 500, closed symbols) and two operational cycles (1 and 2). Nominal radiation level, 25 ccH_2/kg, 300 °C, *Re* = 1000 and *W* = 10 μm.

the amount needed increasing slightly with the dose rate. Concentrations at the mouth are plotted for they adequately show the suppression of radiolysis by primary water hydrogen and the concentrations are anyway lower inside the crevice.

Figs. 8 and 9 show the dissolved hydrogen concentration at the crevice mouth and tip, respectively, as a function of the primary water hydrogen concentration for various crevice aspect ratios and radiation levels. At low primary water hydrogen concentration the bulk dissolved hydrogen concentration is determined by radiolytic production (concentrations above the 1-to-1 line). From the point where the primary water hydrogen starts to suppress radiolysis (0.1–1 ccH_2/kg), the bulk dissolved hydrogen concentration is determined by the primary water hydrogen concentration. Inside the crevice and especially at the tip of a large aspect ratio crevice (Fig. 9) the hydrogen ion concentration (due to metal cation hydrolysis) and, subsequently, (due to the hydrogen evolution reaction), the dissolved hydrogen concentration increase significantly. This leads to enhanced suppression of radiolysis inside the crevice.

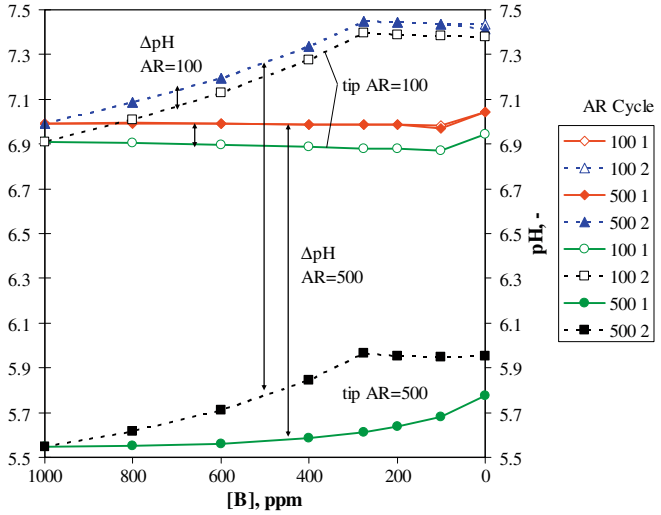

Fig. 13. pH at crevice mouth (diamonds and triangles) and tip (circles and squares) as a function of boric acid concentration for two crevice aspect ratios (100, open symbols and 500, closed symbols) and two operational cycles (1 and 2). Nominal radiation level, 25 ccH_2/kg, 300 °C, $Re = 1000$ and $W = 10$ μm.

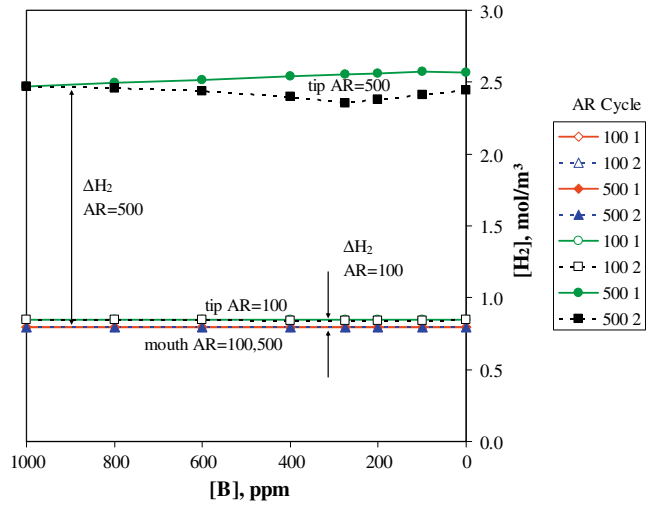

Fig. 15. Dissolved hydrogen concentration at the crevice mouth (diamonds and triangles) and tip (circles and squares) as a function of boric acid concentration for two crevice aspect ratios (100, open symbols and 500, closed symbols) and two operational cycles (1 and 2). Nominal radiation level, 25 ccH_2/kg, 300 °C, $Re = 1000$ and $W = 10$ μm.

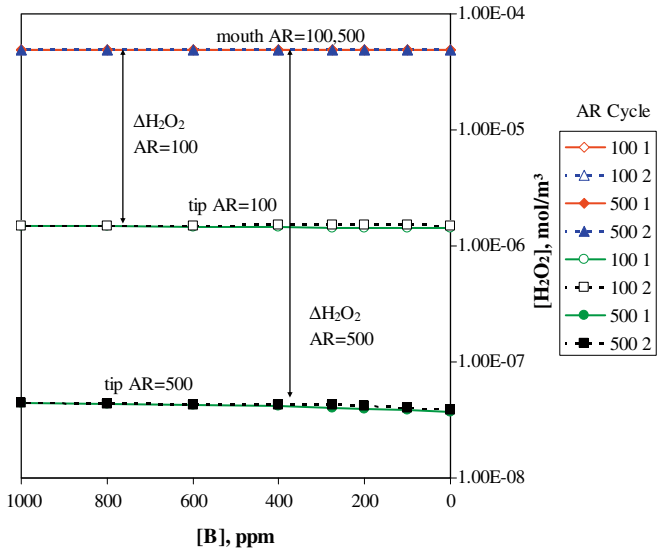

Fig. 14. Hydrogen-peroxide concentration at the crevice mouth (diamonds and triangles) and tip (circles and squares) as a function of boric acid concentration for two crevice aspect ratios (100, open symbols and 500, closed symbols) and two operational cycles (1 and 2). Nominal radiation level, 25 ccH_2/kg, 300 °C, $Re = 1000$ and $W = 10$ μm.

Figs. 3–9 show that radiolysis is being suppressed between a primary water hydrogen concentration of 0.1 and 1 ccH_2/kg, the actual value depending a bit on the crevice aspect ratio and the radiation level.

To avoid a corrosion potential higher than $-230\ mV_{she}$ (often quoted to avoid SCC in light water reactors [9]) a primary water hydrogen concentration above 20 ccH_2/kg is to be maintained in respect of the studied crevices (Figs. 2 and 4), which corresponds well with the values used in operation, i.e. 25 ccH_2/kg. Looking at the graphs of dissolved oxygen (Fig. 6) and hydrogen peroxide (Fig. 7), a primary water hydrogen concentration of a few ccH_2/kg would be sufficient to suppress their radiolytic yield, which is in agreement with literature [10]. However, the pH results (Fig. 5) show that in the case of a long crevice ($L/W = 500$, $W = 10$ μm) the primary water hydrogen concentration needs to exceed 50 ccH_2/kg. Indeed, the pH drop into the crevice is about 1–2 units. This could have a significant effect on SCC initiation and subsequent propagation; as can be anticipated from glancing at oxide stability domains in a Pourbaix diagram. If plants do have a problem with SCC initiation, and this is associated with long crevices, then, a possible mitigation could be to move to a higher primary water hydrogen concentration than the standard 25–35 ccH_2/kg, for this would increase the tip pH. Of course this would require further efforts in quantifying the effect of pH on SCC initiation and an evaluation of whether the increased primary water hydrogen concentration is not exacerbating other potential plant issues.

5.2. Effect of the boric acid–lithium hydroxide cycle

Fig. 11 shows the corrosion potential as a function of the total boron concentration for two crevice aspect ratios and two operational cycles. The constant pH cycle (cycle 1) seems to have a slightly, but insignificantly, higher corrosion potential (Fig. 11). Overall, the corrosion potential is independent of the total boron-lithium concentration variations throughout both of the operational cycles.

Fig. 12 shows the electrode potential at the crevice mouth and tip as a function of the total boron concentration for two crevice aspect ratios and two operational cycles. The electrode potential at the mouth of the crevice is close to the corrosion potential. There is a potential drop into the crevice which, for the larger aspect ratio crevice, is of the order of 150 mV at the tip of the crevice. The potential drop into the crevice is almost independent of the total boron–lithium concentration variations throughout both of the operational cycles.

Fig. 13 shows the pH at the crevice mouth and tip as a function of the total boron concentration for two crevice aspect ratios and two operational cycles. The pH at the mouth of the crevice follows closely the cycles' pH. There is a pH drop into the crevice which, for the larger aspect ratio crevice, is of the order of one pH unit at the tip of the crevice. This could be significant in respect of stress corrosion cracking.

Fig. 14 shows the hydrogen-peroxide concentration at the crevice mouth and tip as a function of the total boron concentration for two crevice aspect ratios and two operational cycles. The

hydrogen-peroxide concentration at the mouth of the crevice is hardly influenced by the cycle or the aspect ratio (top curves all falling on top of each other). There is a hydrogen-peroxide concentration drop into the crevice. Since radiolysis has been modelled in the crevice's internal and external environments, this drop shows that radiolysis happens to a smaller extend in tight crevices (see further).

Fig. 15 shows the dissolved hydrogen concentration at the crevice mouth and tip as a function of the total boron concentration for two crevice aspect ratios and two operational cycles. The dissolved hydrogen concentration at the mouth of the crevice is hardly influenced by the cycle or the aspect ratio (bottom curves all falling on top of each other) and is close to the primary water hydrogen concentration (25 $ccH_2/kg = 0.8\ mol/m^3$). There is an increase of the dissolved hydrogen concentration into the crevice which, for the large aspect ratio crevice, is of the order of 50 ccH_2/kg at the tip of the crevice. This probably further suppresses radiolysis, simultaneously lowering the hydrogen-peroxide concentration as discussed in the previous graph.

In conclusion, the differences between the two operational cycles are probably insignificant, whereas the aspect ratio of the crevice is an important factor in respect of the local conditions at the tip of the crevice.

6. Conclusions

Local electrochemical conditions within crevices are important in respect of stress corrosion cracking, initiation and propagation. A finite element model has been developed to calculate the local crevice conditions taking into account the effect of water radiolysis. This model is encompassed in ECHEM, a user-oriented tool to calculate the electrochemical conditions within 2D, rectangular, 316 stainless steel crevices. Sensitivity studies have been performed using this model, yielding the following conclusions:

- The model predicts that a primary water hydrogen concentration of just over 20 $ccH_2/kg(STP)$ is sufficient to remain below an electrode potential of $-230\ mV_{she}$, a guideline value commonly used with respect to stress corrosion cracking in BWR's.
- The model predicts that a primary water hydrogen concentration of around 50 $ccH_2/kg(STP)$ is needed in order to avoid a pH drop of the order of 1–2 units inside the crevice. Such a large pH drop would likely have a negative effect on stress corrosion crack initiation and propagation.
- Radiolysis affects the local chemistry conditions inside short corroding crevices. However, the model shows that hydrolysis significantly reduces radiolysis inside high aspect ratio corroding crevices.
- The type of operational cycle (constant pH or constant lithium) does not significantly influence the local electrochemical conditions within the crevice. Furthermore, the conditions are almost independent of the total boron–lithium concentration variations throughout both of the operational cycles.

Acknowledgements

The work has been sponsored by SCK•CEN, Tractebel under Contract No. KNT 90991165 and the European Union's integrated 6th Framework Project PERFECT under Contract No. FI6O-CT-2003-508840. The end product, ECHEM, was a collaboration between SCK•CEN (Belgian Nuclear Energy Research Centre) and VUB (Vrije Universiteit Brussel).

References

[1] P.M. Scott, Corrosion 56 (8) (2000) 771.
[2] G.S. Was, P. Andresen, Corrosion 63 (1) (2007) 19.
[3] P.M. Scott, M.C. Meunier, D. Deydier, S. Sylvestreand, A. Trenty, An analysis of Bafle/Former bolt cracking in French PWR, in: Environmentally assisted cracking: Predictive methods for risk assessment and evaluation of materials, ASTM 1401.
[4] A. Turnbull, Corros. Sci. 39 (1997) 789.
[5] J.S. Newman, Electrochemical Systems, 2nd Ed., Prentice-Hall, 1991.
[6] G. Nelissen, G. Weyns, P. Maciel, J. Deconinck, O. Vande Vyver, H. Deconinck, Electrochim. Acta 52 (23) (2007) 6584.
[7] M. Vankeerberghen, Will finite-element analysis find its way to the design against stress corrosion cracking, in: S. Shipilov, R.H. Jones, J.-M. Olive, R. Rebak (Eds.), Environment-induced Cracking of Materials, Elsevier, 2008, ISBN: 978-0-08-044693-6.
[8] M. Jürgensen, H. Neder, D. Wolter, U. Staudt, S. Odar, V. Schneider, VGB Guideline for the Water in Nuclear Power Plants with Light Water Reactors (PWR) VGB-R 401 J, 2006.
[9] F.P. Ford, Corrosion in Boiling Water Reactors, ASM Handbook, Corrosion: Environments and Industries, vol. 13C, 2006, ISBN: 978-0-87170-709-3.
[10] K. Garbett, J. Henshaw, H.E. Sims, Hydrogen and oxygen behaviour in PWR primary coolant, in: Proceedings of the 8th International Conference of Water Chemistry of Nuclear Reactor Systems, Bournemouth, UK, 2000, pp. 85–92.
[11] C.F. Baes, R.E. Mesmer, The Hydrolysis of Cations, John Wiley, New York, 1976.
[12] PWR Primary Water Chemistry Guidelines, Revision 2, EPRI-NP-7077, 1990.
[13] D.D. Macdonald, Private communication.
[14] M. Vankeerberghen, S. Gavrilov, J. Nucl. Mater. 377 (2) (2008) 331.
[15] D.D. Macdonald, M. Urquidi-Macdonald, Corros. Sci. 32 (1) (1991) 51.
[16] T.K. Yeh, D.D. Macdonald, A.T. Motta, Nucl. Sci. Eng. 121 (1995) 468.
[17] P.F. Ford, D.F. Taylor, P.L. Andresen, R.G. Ballinger, Corrosion-assisted Cracking of Stainless Steel and Low Alloy Steels in LWR Environments, EPRI-NP-5064M, 1987.
[18] H. Christensen, Fundamental Aspects of Water Coolant Radiolysis, 2006, ISRN: SKI-R-06/16-SE, ISSN: 1104-1374.
[19] J. Henshaw, Nexia Solutions, vol. 6265, 2005.